

Heterometallic Palladium(II)–Indium(III) and –Gallium(III) Acetate-Bridged Complexes: Synthesis, Structure, and Catalytic Performance in Homogeneous Alkyne and Alkene Hydrogenation

Igor P. Stolarov,[†] Ilya A. Yakushev,[†] Andrei V. Churakov,[†] Natalia V. Cherkashina,[†] Nadezhda S. Smirnova,[†] Evgeny V. Khramov,[‡] Yan V. Zubavichus,[‡] Victor N. Khrustalev,^{‡,§} Alexander A. Markov,[†] Alla P. Klyagina,[†] Alexey B. Kornev,^{||} Vyacheslav M. Martynenko,^{||} Alexander E. Gekhman,[†] Michael N. Vargaftik,^{*,†} and Ilya I. Moiseev[†]

[†]Kurnakov Institute of General and Inorganic Chemistry, Russian Academy of Sciences, Moscow, Russian Federation

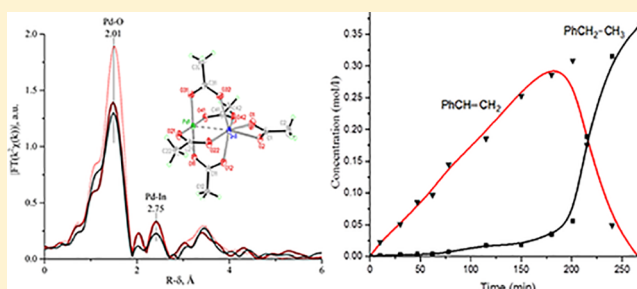
[‡]National Research Center, Kurchatov Institute, Moscow, Russian Federation

[§]Peoples' Friendship University of Russia (RUDN University), Moscow, Russian Federation

^{||}Institute of Problems of Chemical Physics, Russian Academy of Sciences, Chernogolovka, Moscow, Russian Federation

Supporting Information

ABSTRACT: The reaction of $\text{Pd}_3(\text{OOCMe})_6$ with indium(III) and gallium(III) acetates was studied to prepare new Pd^{II} -based heterometallic carboxylate complexes with group 13 metals. The heterometallic palladium(II)–indium(III) acetate-bridged complexes $\text{Pd}(\text{OOCMe})_4\text{In}(\text{OOCMe})$ (**1**) and $\text{Pd}(\text{OOCMe})_4\text{In}(\text{OOCMe})\cdot\text{MeCOOH}$ (**1a**) were synthesized and structurally characterized with X-ray crystallography and extended X-ray absorption fine structure in the solid state and solution. A similar Pd–Ga heterometallic complex formed by the reaction of $\text{Pd}_3(\text{OOCMe})_6$ with gallium(III) acetate in a dilute acetic acid solution, as evidenced by atmospheric pressure chemical ionization mass and UV–vis spectrometry, was unstable at higher concentrations and in the solid state. Complex **1** catalyzes the liquid-phase-selective phenylacetylene and styrene hydrogenation (1 atm of H_2 at 20 °C) in acetic acid, ethyl acetate, and *N,N*-dimethylformamide solutions, while no Pd metal was formed until alkyne and alkene hydrogenation ceased.



1. INTRODUCTION

Currently, multimetallic,^{1a} particularly heterobimetallic Pd^{II} - and Pt^{II} -based complexes, are attracting increasing attention as single-molecular precursors to the mixed-metal nanoparticles and heterogeneous catalysts.^{1b–g} Unlike this, such heterobimetallic complexes are less commonly used as unsupported homogeneous catalysts.² Recently, we found unexpectedly that the unsupported heterobimetallic acetate-bridged complexes $\text{Pt}^{\text{II}}(\mu\text{-OOCMe})_4\text{M}^{\text{II}}(\text{HOOCMe})_4$ ($\text{M} = \text{Ca}, \text{Sr}, \text{Ba}$) efficiently catalyze partial alkyne hydrogenation in the liquid phase.^{3a} A similar catalytic effect was also found for the earlier synthesized Pd-based analogues $\text{Pd}^{\text{II}}(\mu\text{-OOCMe})_4\text{M}^{\text{II}}(\text{HOOCMe})_4$ ($\text{M} = \text{Ca}, \text{Sr}, \text{Ba}$).^{3b} In this work, we attempted to extend the range of complementary to Pd^{II} metals with group 13 elements in view of the expected catalytic potential of new Pd^{II} -based heterometallic complexes. One example of such complexes, $\text{Pd}(\text{OOCMe})_4\text{Tl}(\mu\text{-OOCMe})$, has been reported,^{4a,b} whereas the Pd^{II} -based carboxylates with In^{III} and Ga^{III} were unknown.

2. RESULTS AND DISCUSSION

2.1. UV–Vis Observation of Complexation. Normally, indium(III) and gallium(III) triacetates are poorly soluble in acetic acid. We found that $\text{In}(\text{OOCMe})_3$ and $\text{Ga}(\text{OOCMe})_3$ readily dissolve in glacial acetic acid containing $\text{Pd}_3(\text{OOCMe})_6$ upon stirring at 60–80 °C. The reaction is accompanied by systematical changes in time of the UV–vis spectrum of the solution (Figure 1a–c).

These observations implied complexation of palladium(II) acetate with indium(III) and gallium(III) acetates. The reaction with indium(III) acetate proceeds to completion (Figure 1a). Unlike this, the reaction with gallium(III) acetate observable at low concentrations (Figure 1b) is not completed at higher concentrations (Figure 1c), preventing preparation of the crystalline heterometallic complex (see below).

2.2. Mass Spectrometry (MS) Data. Additional evidence of the formation of the Pd-based heterometallics with indium(III) and gallium(III) acetates gave MS analysis of the products

Received: May 16, 2018

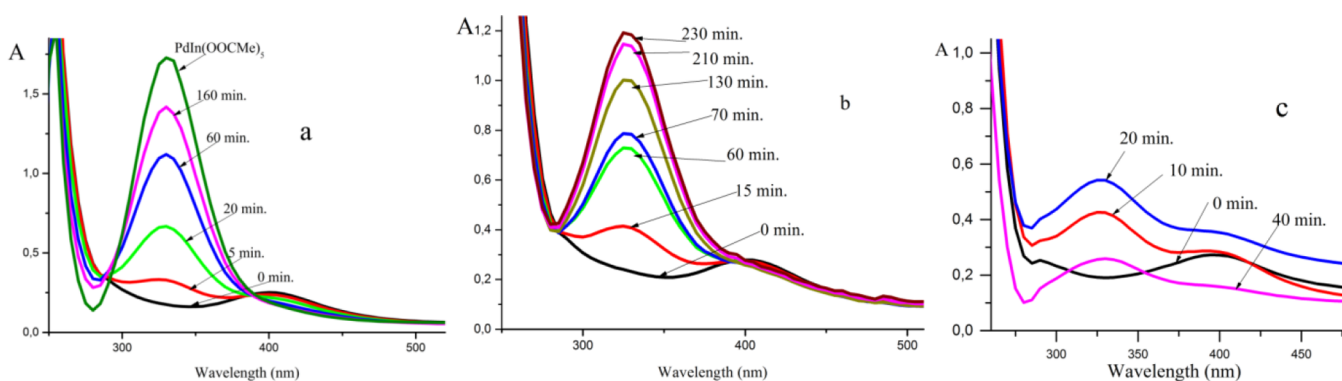


Figure 1. Time profiles of the UV-vis spectra of the reaction solutions [Pd:In (Ga) = 1:1; glacial acetic acid; 80 °C]: (a) $(\text{Pd}_3(\text{OOCMe})_6 + \text{In}(\text{OOCMe})_3, 0.965 \times 10^{-3} \text{ mol L}^{-1}$ each; (b) $(\text{Pd}_3(\text{OOCMe})_6 + \text{Ga}(\text{OOCMe})_3, 0.965 \times 10^{-3} \text{ mol L}^{-1}$ each; (c) reaction at high $(\text{Pd}_3(\text{OOCMe})_6 + \text{Ga}(\text{OOCMe})_3$ concentrations, $21 \times 10^{-3} \text{ mol L}^{-1}$ each (reaction solution probes diluted with acetic acid to $0.462 \times 10^{-3} \text{ mol L}^{-1}$ for spectral recording).

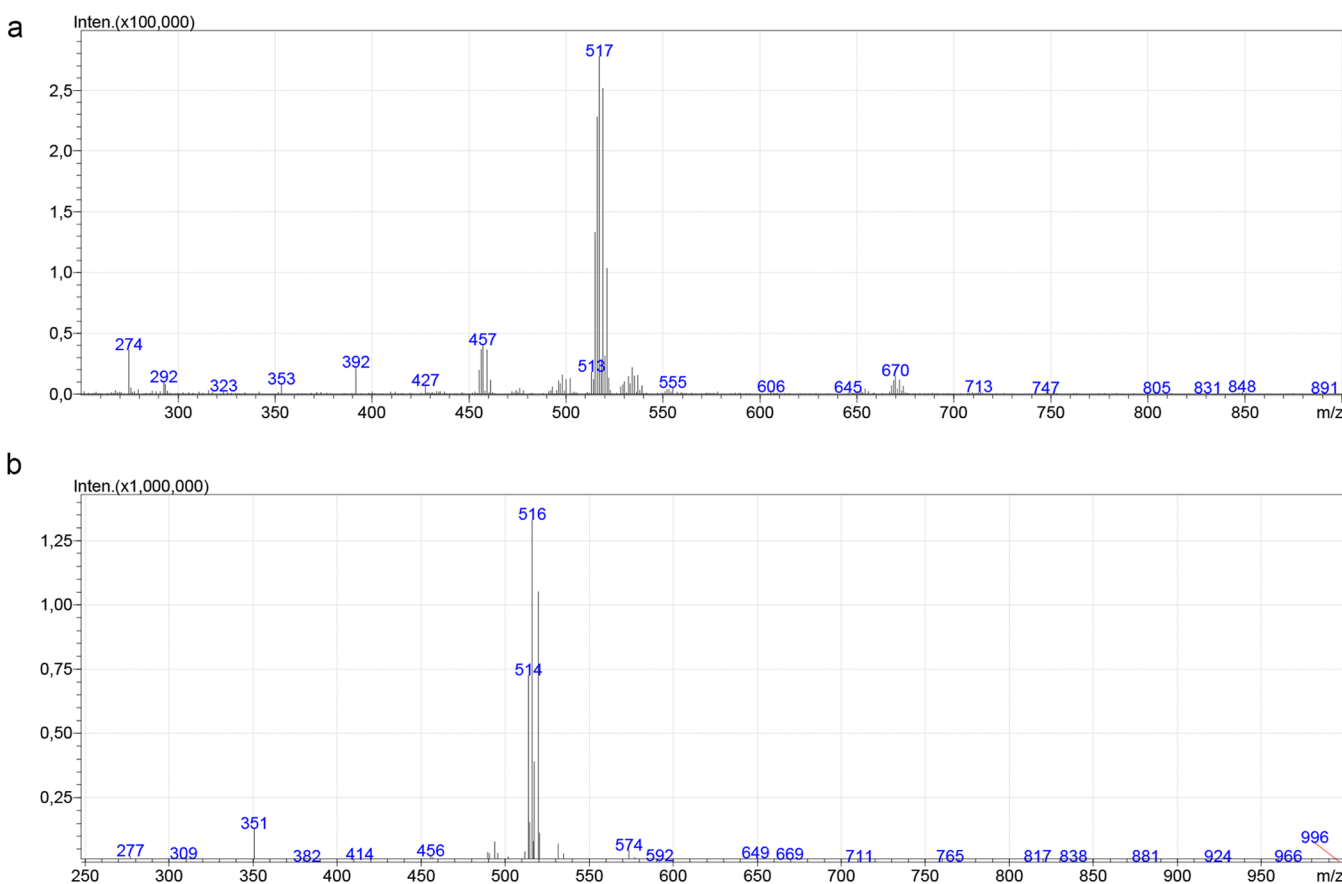


Figure 2. (a) Positive region of the APCI-MS spectrum of the $\text{Pd}_3(\text{OOCMe})_6 + \text{In}(\text{OOCMe})_3$ reaction product. (b) Negative region of the APCI-MS spectrum of the $\text{Pd}_3(\text{OOCMe})_6 + \text{In}(\text{OOCMe})_3$ reaction product.

of the Pd + In (Ga) reaction. The atmospheric pressure chemical ionization MS (APCI-MS) spectrum of the product of the Pd + In reaction in acetic acid revealed a high-intensity isotope cluster with a maximum at m/z 517 in the positive region corresponding to the protonated complex $\text{PdIn}(\text{OOCMe})_5\text{H}^+$ and a smaller isotope cluster with a maximum at m/z 457 corresponding to the heterometallic ion $\text{PdIn}(\text{OOCMe})_4^+$ (Figure 2a).

The negative region (Figure 2b) contains the main peak at m/z 516 corresponding to the ion $\text{PdIn}(\text{OOCMe})_5^-$ and the low-intensity peak at m/z 351 corresponding to the ion $\text{In}(\text{OAc})_4^-$.

The APCI-MS spectrum of the product of the Pd + Ga reaction in acetic acid detected an isotope cluster with a

maximum at m/z 473 in the positive region corresponding to the protonated molecule $\text{PdGa}(\text{OOCMe})_5\text{H}^+$ (Figure 3a).

The negative region (Figure 3b) contains the main peak at m/z 473 corresponding to the ion $\text{PdGa}(\text{OOCMe})_5^-$.

2.3. Preparation of the Heterometallic Complexes. The reaction between $\text{Pd}_3(\text{OOCMe})_6$ and $\text{In}(\text{OOCMe})_3$ in glacial acetic acid produced the crystalline complex $\text{Pd}(\text{OOCMe})_4\text{In}(\text{OOCMe})\cdot\text{HOOCMe}$ (**1a**) as the crystal solvate in the yield 49% based on Pd. Recrystallization of **1a** from benzene produced the solvent-free complex $\text{Pd}(\text{OOCMe})_4\text{In}(\text{OOCMe})$ (**1**) in the yield 36% based on Pd. Both **1** and **1a** were

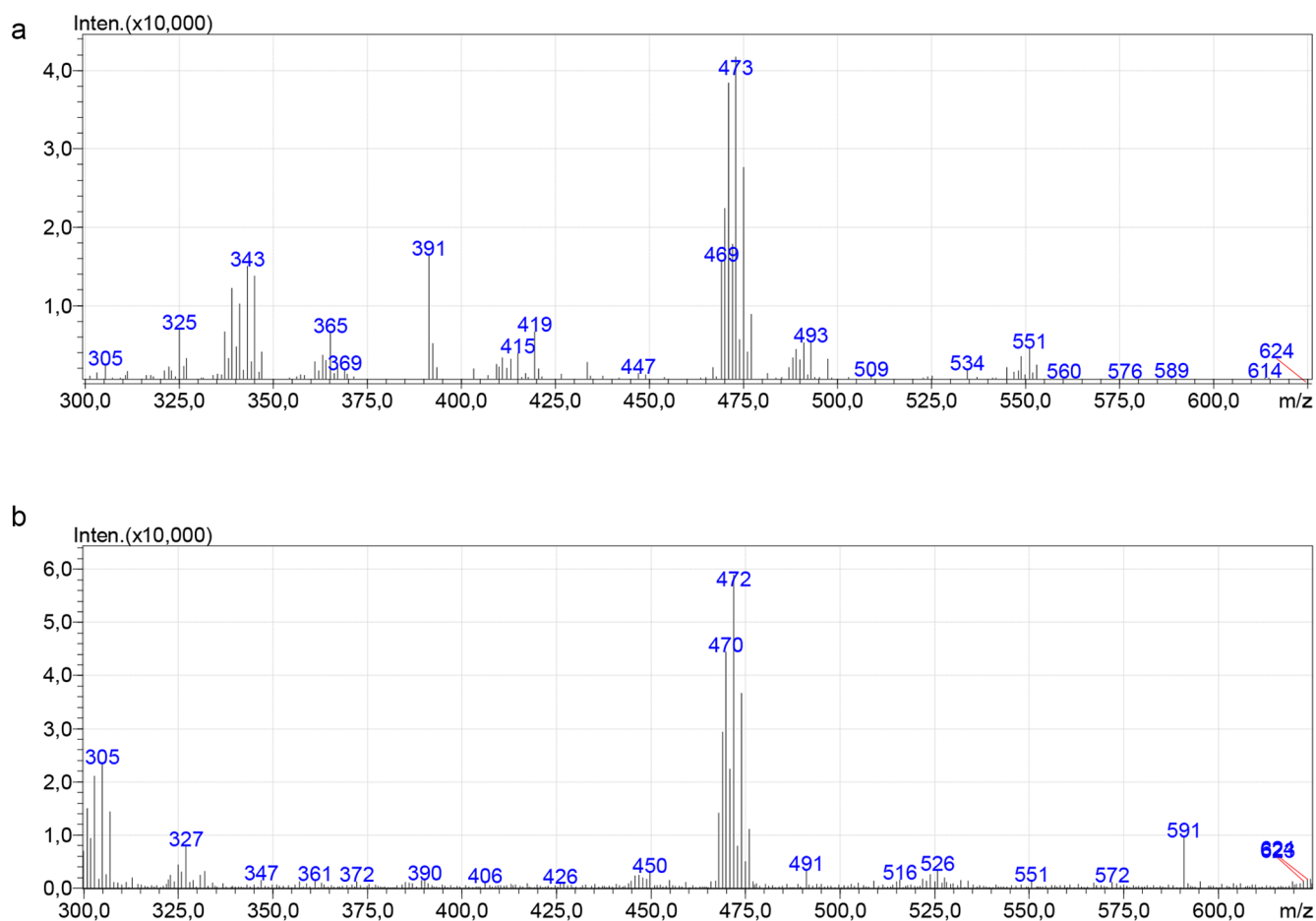


Figure 3. (a) Positive region of the APCI-MS spectrum of the $\text{Pd}_3(\text{OOCMe})_6 + \text{Ga}(\text{OOCMe})_3$ reaction product. (b) Negative region containing the main peak at m/z 473 corresponding to the ion $\text{PdGa}(\text{OOCMe})_5^-$.

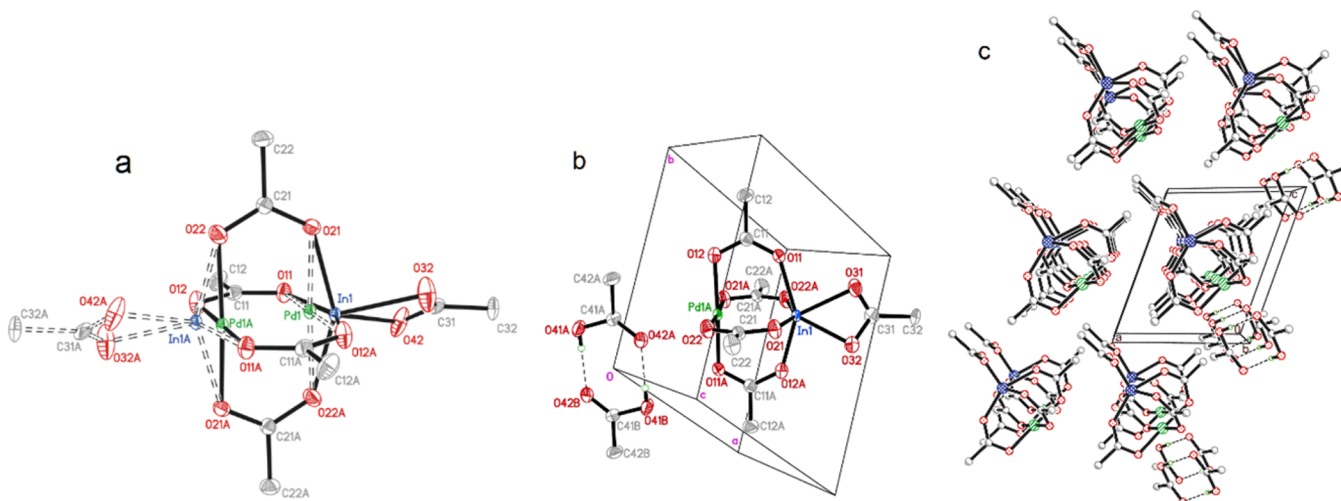


Figure 4. (a) Molecular structure of complex **1a** showing disordering of the Pd and In surroundings. (b) Structure of complex **1** with solvation acetic acid molecules. Displacement ellipsoids are shown at the 35% probability level (H atoms are omitted for clarity; for crystal data and structure refinement, see Table 3). (c) Crystal packing of complex **1a**.

structurally characterized with X-ray crystallography (see below).

Unlike this, palladium(II)–gallium(III) complexation through the reaction of $\text{Pd}_3(\text{OOCMe})_6$ with $\text{Ga}(\text{OOCMe})_3$ was observed only in a fairly dilute ($\sim 10^{-3}$ mol L^{-1}) acetic acid

solution, which was evidenced by UV–vis spectrometry and APCI-MS (see sections 2.1 and 2.2). However, numerous attempts to concentrate the reaction solution for isolation of the crystalline palladium(II)–gallium(III) heterometallic complex were unsuccessful.

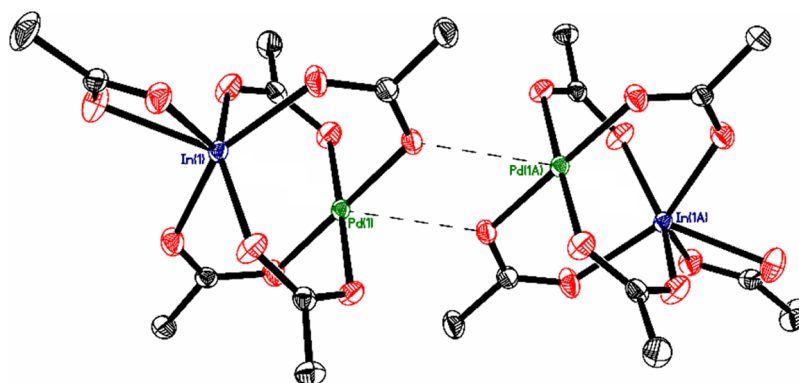


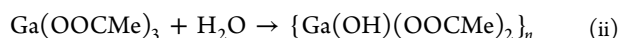
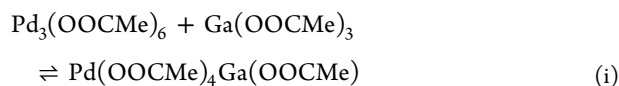
Figure 5. Molecular structure of complex **1** with displacement ellipsoids shown at the 50% probability level (H atoms are omitted for clarity; for crystal data and structure refinement, see Table 3).

Table 1. Selected Geometric Parameters of Complexes PdM(OOCMe)₅ (M = Ga, In, Tl) in Angstroms

complex	method	Pd–O _{eq}	Pd–M	M–O _{eq} ^a	M–O _{ax} ¹	M–O ²	ref
PdGa(OAc) ₅	PBE0/def2-SVP	2.007	2.674	1.990 ± 0.008	1.833	3.041	
	PBE0/MCP-TZP	2.019	2.637	1.960 ± 0.010	1.800	3.035	
	M06/def2-SVP	2.029	2.710	1.987 ± 0.009	1.825	2.998	
PdIn(OAc) ₅	PBE0-D3/MCP-TZP	2.017 ± 0.001	2.641	1.960 ± 0.010	1.799	3.021	
	PBE0/def2-SVP	2.005 ± 0.002	2.790	2.213 ± 0.007	2.171	2.322	
	PBE0-D3/MCP-TZP	2.016 ± 0.003	2.760	2.180 ± 0.010	2.124	2.285	
PdTl(OAc) ₅	exp. XRD	1.995(3)–2.119(3)	2.7438(2)	2.060(3)–2.200(3)	2.186(7)	2.248(1)	this work
	PBE0/def2-SVP	2.003 ± 0.001	2.781	2.323 ± 0.006	2.242	2.406	
	PBE0/MCP-TZP	2.015 ± 0.002	2.746	2.278 ± 0.009	2.189	2.368	
	PBE0-D3/MCP-TZP	2.014 ± 0.002	2.750	2.273 ± 0.009	2.187	2.362	
	exp. XRD	2.003(7)	2.702	2.269(14)	2.249	2.353	4b

^aMean values are shown with mean absolute deviations.

The failure origin is not clear. Most likely, this is due to the known tendency of gallium(III) salts, particularly gallium(III) acetate, to form unreactive, poorly dissolved gallium hydroxo complexes through hydrolytic polymerization:^{5a–c}



In the synthesis, stage (i) seems to be reversible. Seemingly, irreversible hydrolytic stage (ii) removes gallium(III) acetate when the water content, even in the thoroughly dehydrated (≤ 0.05 wt %) glacial acetic acid, is sufficient to shift left the equilibrium stage (i). This obstacle was insignificant at the initial period of the reaction at low reactant concentration (Figure 1b), while it became prevailing in the synthetic runs at higher gallium acetate concentration (Figure 1c) probably because of reaction (ii) acceleration. We met the more hydrolytic confinement in an attempt to prepare the acetate-bridged palladium(II)–

aluminum(III) heterometallic complex by the reaction of Pd₃(OOCMe)₆ with Al(OOCMe)₃.

Hence, further studies were performed with the palladium(II)–indium(III) complex **1**.

2.4. X-ray Crystallography of 1 and 1a. The molecular structure of complex **1a** was determined with two parallel single-crystal X-ray diffraction (XRD) techniques: (1) larger crystals (0.20 × 0.16 × 0.06 mm) were studied using a Bruker SMART Apex II laboratory diffractometer (Center of Shared Equipment of the Kurnakov Institute) and (2) smaller crystals (0.15 × 0.07 × 0.04 mm) were studied on the Belok beamline of the Kurchatov Synchrotron Radiation Source at the National Research Center, Kurchatov Institute (Moscow, Russian Federation). Both crystals **1** and **1a** were prepared in independent synthetic runs, and the results of both experiments are very close each other.

Analysis of the Fourier electron density synthesis for crystal **1a** revealed that the metal atoms are disordered over two positions with nearly equal occupancies (Figure 4a). The distance between two positions in structure **1a** is approximately 0.6 Å.

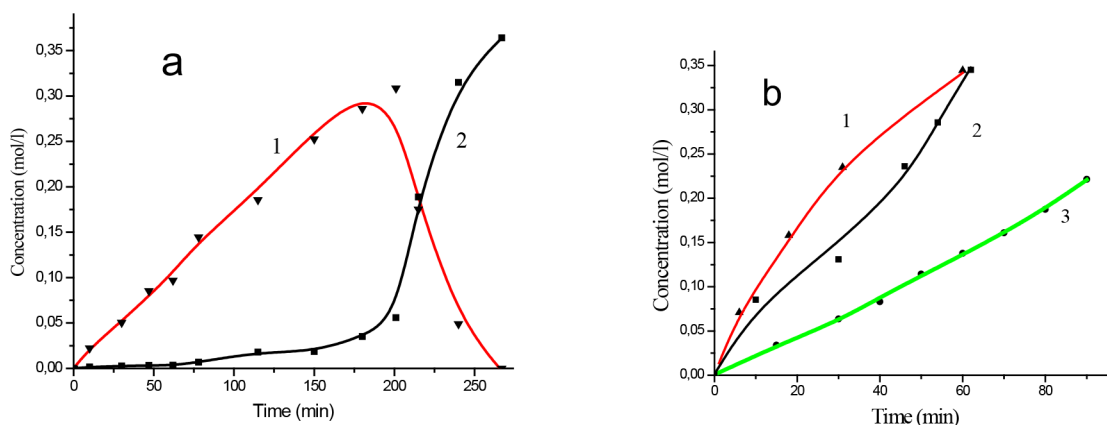


Figure 6. (a) Time profile for phenylacetylene hydrogenation (1 atm of H_2 at $20^\circ C$; $PhC\equiv CH$ initial concentration 0.36 mol L^{-1}) in $0.4 \times 10^{-3}\text{ mol L}^{-1}$ of complex **1** in an acetic acid solution: styrene accumulation (curve 1, red curve) and ethylbenzene accumulation (curve 2, black curve). (b) Time profile for styrene-to-ethylbenzene hydrogenation (1 atm of H_2 at $20^\circ C$; $PhCH=CH_2$ initial concentration 0.35 mol L^{-1}) in a $0.2 \times 10^{-3}\text{ mol L}^{-1}$ solution of complex **1** in different solvents: 1, acetic acid (red curve); 2, ethyl acetate (black curve); 3, DMF (green curve).

The crystal cell contains one disordered complex molecule with a solvated acetic acid molecule, as shown in Figure 4a–c.

The solvent-free complex **1** was prepared by recrystallization of **1a** from dry benzene. The structure of crystal **1** ($0.25 \times 0.20 \times 0.02\text{ mm}$) was studied with a Bruker SMART Apex II diffractometer. The crystal cell contains one crystallographically independent complex molecule without disorder, with relatively short contact between the Pd and O atoms of the bridging acetic group of adjacent molecule **1** [$2.8361(2)\text{ \AA}$].

The heterometallic molecule $Pd(\mu\text{-OOCMe})_4In(\text{OOCMe})$ in crystals **1a** and **1** has a paddlewheel structure (Figure 5) similar to that of the precedential palladium(II)–thallium(III) complex $Pd(\text{OOCMe})_4Tl(\mu\text{-OOCMe})$.^{4a,b}

In both structures, the Pd–O, In–O, C–O, and Pd–In interatomic distances are almost identical with each other and the Pd atoms have a square-plane environment [distortion from the O plane: $0.005(1)$ – $0.038(2)\text{ \AA}$ in **1** and **1a**] of four O atoms belonging to the bridging acetate ligands connecting to the Pd and In atoms [Pd–O $1.995(3)$ – $2.119(3)\text{ \AA}$; In–O $2.060(3)$ – $2.200(3)\text{ \AA}$]. The In atom has a six-coordinated environment in **1** [In–O $2.186(7)$ – $2.248(13)\text{ \AA}$] with the terminal acetate group and a rather short Pd–In distance [$2.7438(2)\text{ \AA}$].

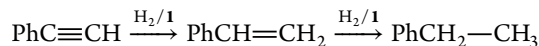
2.5. Density Functional Theory (DFT) Calculations of $PdM(\text{OOCMe})_5$ ($M = Ga, In, Tl$). The equilibrium structure of $PdGa(\text{OOCMe})_5$ acetate-bridged complex was calculated at various computational levels (Table 1; see section 3.2.3 for computational details). According to the calculations, the interatomic distances $R(Ga-O_{eq})$ are significantly shorter (by 0.03 – 0.07 \AA) than those in the other heterobimetallic complexes. Similarly, the distance $R(Pd-Ga)$ is also the shortest among the considered complexes. Another feature of complex $PdGa(\text{OOCMe})_5$ is monodentate coordination of the acetate ligand. We were unable to calculate the equilibrium geometry of $PdIn(\text{OOCMe})_5$ with the M06 functional and at PBE0/MCP-TZP level, but the data obtained using the dispersion-corrected PBE0 functional are in satisfactory agreement with the experimental data. The same can be said with some caution for complex $PdTl(\text{OOCMe})_5$. The calculated distance $R(Pd-Tl)$ in the equilibrium structures is significantly longer, by 0.04 – 0.08 \AA , compared to the XRD data.

2.6. Catalysis in Homogeneous Hydrogenation. Earlier we synthesized and structurally characterized a series of crystalline Pd^{II} -based heterometallic carboxylate complexes

with 3d transition^{6a–e} and 4f rare-earth and alkaline-earth metals.^{3a,7a–d} Some of these complexes were successfully practiced as precursors to supported catalysts for hydrogenation, reductive dehydration, and other gas-phase and liquid-phase reactions.^{8a–h}

In this work, we unexpectedly found that unsupported complex **1** catalyzes itself the partial alkyne and alkene hydrogenation with H_2 in the liquid phase. Generally, monometallic palladium(II) complexes are easily reduced to metallic Pd just by feeding of gaseous H_2 , whereas the catalytic reaction proceeds over metallic Pd.^{9a–c}

We also found that complex **1** was reduced by H_2 in acetic acid, *N,N*-dimethylformamide (DMF), and other solvents. However, no reduction to Pd metal was observed when phenylacetylene or styrene was preliminarily added to the solution of **1** in acetic acid, ethyl acetate, and DMF, while alkyne hydrogenation proceeded in homogeneous conditions without the formation of Pd metal (Figure 6a,b).



Apparently, phenylacetylene and styrene acted as π ligands, stabilizing an active form of the heterometallic complex. Just after completion of hydrogenation, Pd^{II} was reduced to Pd metal.

In our experiments, the initial rate (turnover frequency, TOF) of styrene-to-ethylbenzene hydrogenation in an acetic acid solution of $Pd_3(\text{OOCMe})_6$ (just after its fast reduction with H_2) was 200 h^{-1} , whereas in the solution of complex **1**, the TOF was at least 2400 h^{-1} .

The catalytic ability of complex **1** is apparently due to the influence of the complementary metal. In the crystal, the Pd and In atoms are positioned at a rather short Pd–In distance, $2.7438(2)\text{ \AA}$. It was of interest what happens upon passage of molecule **1** to a solution in which it displayed catalytic behavior. For this reason, we studied by extended X-ray absorption fine structure (EXAFS) the structural changes in molecule **1** upon transfer from a crystal to a solution.

2.7. EXAFS Study: Comparison of **1 in the Solid State and Solution.** Some information on the behavior of complex **1** in catalytic solutions could give EXAFS data. The Pd K-edge EXAFS spectra showed that the coordination environment of the Pd atom in **1** is retained upon dissolution in benzene and glacial acetic acid (Figure 7).

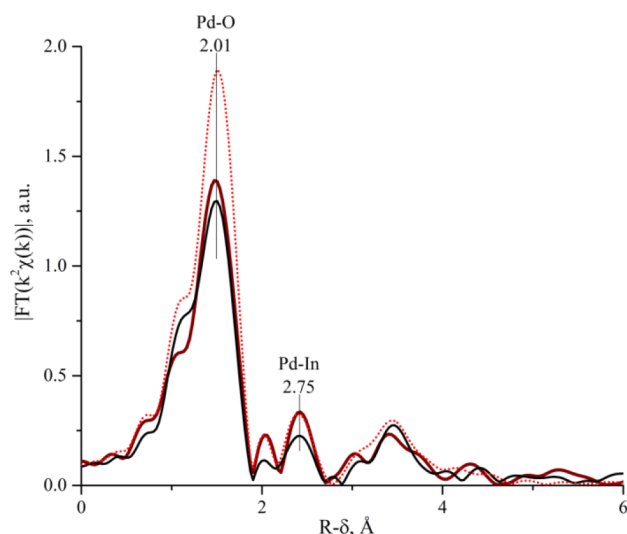


Figure 7. Pd K-edge EXAFS spectra of solid **1** (red dotted curve) and $0.91 \times 10^{-3} \text{ mol L}^{-1}$ solutions of **1** in glacial acetic acid (dark-red solid curve) and benzene (black solid curve).

The atomic radial distribution functions around Pd atoms of the solid **1** and its solutions in benzene and acetic acid have coinciding maxima (Figure 7). The Fourier transforms of EXAFS spectra have three main maxima for all of the samples. The highest maximum corresponds to the coordination sphere of Pd–O. The next peak was attributed to the distance between the Pd and In atoms. The broad peak in the range between 3 and 4 Å (in the $R-\delta$ scale) is related to a set of Pd–O and Pd–C distances.

Simulation of the Fourier transform of the EXAFS spectra for **1** showed that the Pd first coordination sphere has four neighboring O atoms with a mean distance of 2.00 Å. A slight increase in the coordination number for a Pd–O sphere in the model for the solid sample is likely due to some disorder of its structure. The model spectrum of solid **1** also confirms the presence of a single In atom at the distance of 2.73 Å. The fitting results show that dissolution of the complex in benzene or acetic acid does not change noticeably its original structure (Table 2).

Unlike this, the Pd K-edge EXAFS spectrum of **1** in a DMF solution (Figure 8) implies a distortion of the bimetallic structure **1** in this medium, which possibly promotes

Table 2. Results of Modeling of the EXAFS Spectra for Solid 1 and Its Solutions in Acetic Acid and Benzene (R = Interatomic Distance, N = Coordination Number, σ^2 = Debye Factor, and R Factor = Matching Factor between the Experimental and Model Spectra)

scattering pathway	R , Å	N	σ^2 , Å ²	ΔE_0 , eV	R factor, %
Solid 1					
Pd–O	2.00	4.9 ^a	0.001	0.2	2.5
Pd–In	2.73	1.0 ^a	0.010		
Solution of 1 in Acetic Acid					
Pd–O	2.00	4.0 ^a	0.002	0.3	2.0
Pd–In	2.73	1.0 ^a	0.009		
Solution of 1 in Benzene					
Pd–O	1.99	4.0 ^a	0.003	0.2	3.3
Pd–In	2.76	1.0 ^a	0.012		

^aFixed values in modeling.

coordination to Pd atom of the alkene molecule, facilitating its hydrogenation.

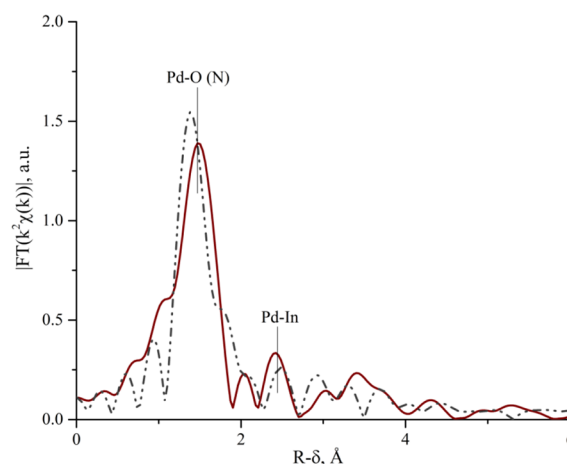


Figure 8. Pd K-edge EXAFS spectra of $0.91 \times 10^{-3} \text{ mol L}^{-1}$ solutions of **1** in DMF (gray thin line) and in glacial acetic acid (dark-red thick line).

Therefore, the mechanism of catalytic hydrogenation in a solution of **1** needs additional investigation.

3. EXPERIMENTAL SECTION

3.1. Reagents and Solvents. Solvents [glacial acetic acid, benzene, DMF, and acetonitrile (all reagent grade, Sigma-Aldrich)] were purified by standard procedures.¹⁰ Glacial acetic acid for synthetic runs was additionally dehydrated by reflux with $\text{B}(\text{OOCMe})_3$, followed by rectification; the water content [gas chromatography (GC) analysis] was at most 0.05%. Gaseous H_2 (high purity, PGS service, Moscow, Russian Federation) was fed at 1 atm from the cylinder through a pressure regulator.

Palladium(II) acetate $\text{Pd}_3(\text{OOCMe})_6$ was prepared by the oxidation of Pd black [prepared by the reduction of PdCl_2 (reagent grade, Reakhim, Russia) with NaBH_4] with concentrated HNO_3 in glacial acetic acid by a known procedure.¹¹ The raw reaction product was purified from the admixture of palladium(II) nitrite complexes by refluxing in glacial acetic acid with a fresh portion of Pd black until NO_2 evolution ceased, followed by recrystallization from hot acetic acid.

Gallium(III) and Indium(III) Acetates. A synthetic difficulty was the high moisture sensitivity and fast aging of these chemicals. For that reason, we used the starting materials prepared according to the following protocols.

Ga(OOCMe)₃. Gallium nitrate $\text{Ga}(\text{NO}_3)_3 \cdot 8\text{H}_2\text{O}$ (4.29 g, 10 mmol) prepared from high-purity gallium oxide (Sigma-Aldrich) was refluxed in 50 mL of acetic anhydride until complete removal of nitrogen oxide (2 h). The solution was evaporated to dryness on a rotary evaporator (1 mm, 70 °C in the bath) and dry-stored in a vacuum desiccator over KOH. Yield: 2.58 g (97.6%). Anal. Calcd for $\text{GaC}_6\text{H}_9\text{O}_6$: C, 29.18; H, 3.65. Found: C, 28.34; H, 4.46. IR (ATR, ν/cm^{-1}): 1700 m, 1630 s, 1535 s, 1440 s, 1405 s, 1342 m, 1317 m, 1235 w, 1049 w, 1026 m, 968 w, 673 s, 632 s, 618 s.

In(OOCMe)₃. Indium nitrate $\text{In}(\text{NO}_3)_3 \cdot 4.5\text{H}_2\text{O}$ (3.818 g, 10 mmol) prepared from high-purity indium oxide (Sigma-Aldrich) was refluxed for 3 h in 50 mL of acetic anhydride until complete removal of nitrogen dioxide. The solution was evaporated to dryness on a rotary evaporator (1 mm, 70 °C in the bath) and dry-stored in a vacuum desiccator over KOH. Yield: 2.850 g (97.5%). The composition corresponds to water-free $\text{In}(\text{OOCMe})_3$. Anal. Calcd for $\text{InC}_6\text{H}_9\text{O}_6$: C, 24.68; H, 3.11. Found: C, 24.83; H, 3.04. FTIR (ATR, cm^{-1}): $\nu_{\text{as}}(\text{COO})$ 1538, $\nu_{\text{s}}(\text{COO})$ 1410.

3.2. Physical Measurements. Elemental analysis (C, H, and N) was performed on an automated $\text{C}_x\text{H}_y\text{N}_z$ -analyzer (EA3000, EuroVector, EU). UV–vis spectrometry was monitored on a Varian Cary 50

spectrophotometer with a standard built-in adjustable Peltier thermostat in a quartz cell (10 mm) with a magnetic stirrer at 25–80 °C (± 0.1 °C). Attenuated-total-reflectance (ATR) IR spectra were recorded on a Nicolet Nexus spectrometer with a Pike micro-ATR accessory.

3.2.1. XRD Analysis. The experimental intensities for **1** and **1a** were collected on a Bruker SMART APEX II and those for **1a** on a Belok beamline of the National Research Center, Kurchatov Institute, using a Rayonix SX165 CCD detector at 150 and 100 K, respectively. Data reductions were performed using SAINT software,¹² and the iMOSFLM utility in the CCP4i package for synchrotron studies.¹³ Absorption corrections based on measurements of equivalent reflections were used.¹⁴ The structures were solved by direct methods and refined by full-matrix least squares on F^2 with anisotropic thermal parameters for all non-H atoms.¹⁵ The In and Pd atoms were found to be disordered over two proximal positions with almost equal occupancies. They were refined with common thermal parameters (EADP). All H atoms were placed in calculated positions and refined using a riding model. Detailed crystallographic data are given in Table 3.

Crystallographic data for **1** and **1a** have been deposited with the Cambridge Crystallographic Data Center (CCDC 1841645–1841647).

3.2.2. MS Characterization. Electrospray and DUIS MS spectra were obtained with a Shimadzu LCMS-2020 instrument (Shimadzu Scientific Instruments, Kyoto, Japan). Samples were dissolved in

acetonitrile immediately before analysis (J. T. Baker, Phillipsburg, NJ; stored over preactivated 4 Å molecular sieves) or glacial acetic acid to a concentration of 0.1 mg mL⁻¹. The solution was directly injected into the mass spectrometer. The heat block was maintained at 150 °C and the desolvation line at 150 °C. Nitrogen was used as the nebulizing and drying gas (1.5 and 15 L min⁻¹, respectively). The electrospray interface voltage was set at 3.0 kV for positive ions and at -3.0 kV for negative ions. The spectral range was m/z 200–2000. Shimadzu LabSolutions software was used for data analysis.

3.2.3. Quantum-Chemical Calculations. The equilibrium geometries of complexes PdM(CH₃COO)₅ (M = Ga, In, Tl) were found using DFT functionals PBE0¹⁶ and M06¹⁷ within spin-restricted formalism. Grimme's empirical dispersion correction scheme D3^{9a} was used in conjunction with the PBE0 functional, as implemented^{18b} in GAMESS-US.¹⁹ The model core potential basis set MCP-TZP²⁰ and Ahlrich's def2-SVP^{21a} all-electron basis set for all atoms, except Pd, for which the effective core potential was employed, were used. The def2-SVP basis set was obtained from EMSL Basis Set Exchange Library.^{21b} All calculations were performed with the GAMESS-US package. We used Jmol²² with POV-Ray software for visualization and figure preparation.

3.2.4. XAFS. The XAFS spectra were measured on the Structural Materials Science beamline on the synchrotron radiation source Sibir-2 at the National Research Center, Kurchatov Institute (Moscow, Russian Federation). The X-ray beam (energy resolution $\Delta E/E \approx 2 \times 10^{-4}$) was monochromatized using a silicon single crystal (220) with the "butterfly" cut-out. The XAFS absorption spectra of Pd K-edge of liquid and solid samples were recorded in transmission mode. The XAFS spectra of solutions were collected in a quartz cuvette with an optical path length of 5 cm. Two ionization chambers filled with argon and xenon were used as detectors. The spectra were processed using the IFEFFIT program package.²³ The modeling of EXAFS spectra was carried out in R space. The Fourier transforms of EXAFS oscillations were taken in a range of $k = 3-12 \text{ \AA}^{-1}$ with the weight coefficient k^2 and approximated in a range of $R = 1.1-2.8 \text{ \AA}$.

3.3. Syntheses. **3.3.1. Pd(μ -OOCMe)₄InOOCMe-AcOH (1a).** A mixture of palladium acetate (224 mg, 1 mmol based on Pd) and indium acetate (292 mg, 1 mmol) was stirred under reflux in 7 mL of glacial acetic acid until a clear yellow-orange solution was formed (0.5 h). The reaction progress was monitored by UV-vis spectrometry of the reaction solution probes. The resulting solution was cooled to room temperature. An orange fine-crystalline precipitate was filtered off, washed with dry ether, and dried in a vacuum desiccator over KOH. Yield of **1a**: 280 mg, 49% based on Pd. Anal. Calcd for PdInC₁₂H₁₉O₁₂: C, 25.00; H, 3.32. Found: C, 25.47; H, 3.50. IR (ATR, ν/cm^{-1}): 3015 br w, 1722 w, 1701 m, 1589 s, 1395 s, 1347 m, 1265 m, 1229 m, 1049 m, 1028 m, 960 w, 922 m, 692 s, 626 s, 606 w, 574 w.

3.3.2. Pd(μ -OOCMe)₄InOOCMe (1). Recrystallization of **1a** from benzene produced the solvent-free complex **1** in a yield of 36% based on Pd. Anal. Calcd for PdInC₁₀H₁₅O₁₀: C, 23.25; H, 2.92. Found: C, 24.02; H, 2.86. IR (ATR, ν/cm^{-1}): 1689 w, 1585 s, 1552 sh, 1445 w, 1414 s, 1396 s, 1351 m, 1296 m, 1047 m, 960 w, 972 m, 694 s, 628 m, 609 w, 593 w, 564 w, 551 m.

Both **1** and **1a** were structurally characterized with X-ray crystallography.

3.3.3. Pd(μ -OOCMe)₄Ga(OOCMe)₂AcOH (2). Palladium acetate (105 mg, 0.47 mmol) and gallium acetate (116 mg, 0.47 mmol) in a mixture of water-free acetic acid containing 0.3% acetic anhydride (40 mL) and *n*-octane (30 mL) and were stirred at 80 °C for 80 min. The reaction progress was monitored by UV-vis spectrometry of the reaction solution probes. The resulting light-yellow solution was filtered off and carefully evaporated almost to dryness on a rotary evaporator with a membrane rotor pump (vacuum 9 Torr, evaporator water bath 20–30 °C, and receiver flask -10 °C). The soggy residue was stored in a fridge (+5 °C) for 12 h, aimed at obtaining the crystalline Pd–Ga complex. As a result, we obtained a yellow amorphous solid containing no crystal phase. The yield of dry **2** is 245 mg (81% based on Pd). Anal. Calcd for PdGaC₁₆H₂₄O₁₆: C, 29.63; H, 3.73. Found: C, 29.55; H, 3.78. IR (ATR, ν/cm^{-1}): 20937 br w, 1713 w, 1599 s, 1566 sh, 1416 s, 1351 m, 1267 w, 1225 w, 1046 m, 973 m, 737 691 s, 671 s, 623 m, 580 w, 561

Table 3. Crystal Data and Structure Refinement for 1a and 1

	1a	1a	1
X-ray source type	fine-focus sealed tube	synchrotron	fine-focus sealed tube
empirical formula	C ₁₂ H ₁₉ InO ₁₂ Pd	C ₁₂ H ₁₉ InO ₁₂ Pd	C ₁₀ H ₁₅ InO ₁₀ Pd
fw	576.49	576.49	516.44
temperature, K	150(2)	100(2)	150(2)
cryst size, mm	0.20 × 0.16 × 0.06	0.15 × 0.07 × 0.04	0.25 × 0.20 × 0.02
wavelength, Å	0.71073	0.96990	0.71073
cryst syst	triclinic	triclinic	triclinic
space group	$P\bar{1}$	$P\bar{1}$	$P\bar{1}$
<i>a</i> , Å	7.2405(8)	7.2309(15)	7.2536(8)
<i>b</i> , Å	8.2457(9)	8.2458(17)	8.7112(10)
<i>c</i> , Å	8.5297(10)	8.5495(17)	12.8212(15)
α , deg	94.6170(10)	94.618(10)	84.983(2)
β , deg	108.447(2)	108.59(2)	84.397(2)
γ , deg	104.6270(10)	104.522(18)	73.875(2)
<i>V</i> , Å ³	460.23(9)	460.51(17)	773.01(15)
<i>Z</i>	1	1	2
density (calcd), Mg mm ⁻³	2.080	2.079	2.219
μ , mm ⁻¹	2.288	5.231	2.701
<i>F</i> (000)	282	282	500
θ range, deg	2.59–27.79	4.244–38.427	2.44–29.00
index range	$-9 \leq h \leq 9, -10 \leq k \leq 10, -11 \leq l \leq 11$	$-9 \leq h \leq 9, -10 \leq k \leq 10, -10 \leq l \leq 10$	$-9 \leq h \leq 9, -11 \leq k \leq 11, -17 \leq l \leq 17$
reflns collected	4762	8131	8607
indep reflns	2215 ($R_{\text{int}} = 0.0108$)	1847 ($R_{\text{int}} = 0.0762$)	4078 ($R_{\text{int}} = 0.0156$)
reflns obsd	2140	1523	3718
R_1/wR_2 [$I > 2\sigma(I)$]	0.0367/0.0840	0.0286/0.0656	0.0180/0.0424
R_1/wR_2 (all data)	0.0375/0.0843	0.0407/0.0711	0.0206/0.0436
GOF on F^2	1.375	1.090	1.050
extinction coeff	0.000	0.0121(17)	0.000
$T_{\text{min}}/T_{\text{max}}$	0.6576/0.8749	0.490/0.802	0.5516/0.9480
$\Delta\rho_{\text{max}}/\Delta\rho_{\text{min}}$, e Å ⁻³	1.120/-0.808	0.481/-0.913	0.575/-0.657

w, 553 w. Numerous synthetic runs attempting isolation of the crystalline complex by varying the reaction conditions resulted in a noncrystalline reaction product only.

3.4. Catalysis. Catalytic experiments were carried out in a glass temperature-controlled (water-jacketed), magnetically stirred flask of 50 mL volume (5 mL of reaction solution, liquid/gas ratio 1:10, and stirring rate 600 rpm). A solution of phenylacetylene (410 mg, 4 mmol) or styrene (208 mg, 2 mmol) in acetic acid, ethyl acetate, or DMF containing complex **1** (1 mg, 0.002 mmol, or 0.5 mg, 0.001 mmol, for phenylacetylene and styrene, respectively) was stirred under H₂ (1 atm) at 20 °C, while the reaction solution remained homogeneous and clear. After 100% styrene conversion, Pd metal sediment and/or a black thin coating on glass appeared. The reaction solution was periodically sampled and monitored by GC (Shimadzu GC-17A, 25 m capillary column, XE-60 phase).

4. CONCLUSIONS

This study was originally intended to challenge the lack of palladium and platinum carboxylate-bridged heterometallics with 13 group metals from In to Al, being encouraged by the earlier successful synthesis of the palladium–thallium acetate from Pd₃(OOCMe)₆ and Tl(OOCMe)₃ by van der Ploeg et al.^{4a} and Balch et al.^{4b} Our experiments showed that only one of the three candidates, indium(III), readily forms a Pd-based acetate-bridged heterometallic complex **1**. An analogous complex with gallium(III) acetate Pd(OOCMe)₄Ga(OOCMe) was detected in a dilute (~10⁻³ mol L⁻¹) acetic acid solution; however, it was not separated as a crystalline solid from more concentrated solutions seemingly because of high hydrolytic susceptibility even at the minor water content (≤0.05%) in glacial acetic acid. We met more hydrolytic obstruction in attempts to prepare a Pd-based complex with aluminum(III) acetate.

The heterometallic Pd–In complex **1** was structurally characterized with X-ray crystallography and EXAFS in the solid state and solution using both the standard laboratory and synchrotron XRD techniques. Unexpectedly, we found that the unsupported complex **1** catalyzes itself in partial phenylacetylene and styrene hydrogenation in the liquid phase, whereas no Pd metal was formed until alkyne and alkene hydrogenation ceased. This fact emphasizes the significant role of supplementary nontransition metals in homogeneous catalysis with noble metals^{24a–c} but needs more detailed investigation.

■ ASSOCIATED CONTENT

Supporting Information

The Supporting Information is available free of charge on the ACS Publications website at DOI: 10.1021/acs.inorgchem.8b01313.

Crystal data and structure refinement for **1a** and **1** (PDF)

Accession Codes

CCDC 1841645–1841647 contain the supplementary crystallographic data for this paper. These data can be obtained free of charge via www.ccdc.cam.ac.uk/data_request/cif, or by emailing data_request@ccdc.cam.ac.uk, or by contacting The Cambridge Crystallographic Data Centre, 12 Union Road, Cambridge CB2 1EZ, UK; fax: +44 1223 336033.

■ AUTHOR INFORMATION

Corresponding Author

*E-mail: wahr36@gmail.com (M.N.V.).

ORCID

Igor P. Stolarov: 0000-0002-3756-7938

Ilya A. Yakushev: 0000-0001-6784-947X

Andrei V. Churakov: 0000-0003-3336-4022

Natalia V. Cherkashina: 0000-0002-5435-2226

Nadezhda S. Smirnova: 0000-0001-6911-0070

Evgeny V. Khramov: 0000-0002-7111-5628

Yan V. Zubavichus: 0000-0003-2266-8944

Victor N. Khrustalev: 0000-0001-8806-2975

Alexander A. Markov: 0000-0002-7035-0490

Alla P. Klyagina: 0000-0003-4326-6573

Alexey B. Kornev: 0000-0002-4217-4063

Vyacheslav M. Martynenko: 0000-0003-0901-0590

Alexander E. Gekhman: 0000-0002-5081-9095

Michael N. Vargaftik: 0000-0001-6574-4906

Ilya I. Moiseev: 0000-0002-8954-7322

Notes

The authors declare no competing financial interest.

■ ACKNOWLEDGMENTS

The authors are thankful for financial support to the Russian Foundation for Basic Research (Projects 17-03-00355, 18-03-00228, and 18-33-00632) and, in part, by the RUDN University Program “5-100”. Synchrotron-radiation-based single-crystal XRD measurements were performed at the unique scientific facility Kurchatov Synchrotron Radiation Source supported by the Ministry of Education and Science of the Russian Federation (Project Code RFMEFI61917X0007).

■ REFERENCES

- (1) (a) Berry, J. F.; Thomas, C. M. Multimetallic complexes: synthesis and applications. *Dalton Trans* **2017**, 46, 5472–5473. (b) Bayot, D. A.; Devillers, M. Precursors Routes for the Preparation of Nb-Based Multimetallic Oxides. In *Progress in Solid State Chemistry Research*; Buckley, R. W., Ed.; Nova Publishers, 2007; pp 117–164. (c) Neo, K. E.; Ong, Y. Y.; Huynh, H. V.; Hor, T. S. A. A single-molecular pathway from heterometallic MM' (M = Ba^{II}, Mn^{II}; M' = Cr^{III}) oxalato complexes to intermetallic composite oxides. *J. Mater. Chem.* **2007**, 17, 1002–1006. (d) Xi, L.; Cho, D. Y.; Duchamp, M.; Boothroyd, C. B.; Lek, J. Y.; Besmehn, A.; Waser, R.; Lam, Y. M.; Kardynal, B. Understanding the Role of Single Molecular ZnS Precursors in the Synthesis of In(Zn)P/ZnS Nanocrystals. *ACS Appl. Mater. Interfaces* **2014**, 6, 18233–18242. (e) Dey, A.; Das, S.; Kundu, S.; Mondal, A.; Rouzières, M.; Mathonière, C.; Clérac, R.; Suriya Narayanan, R.; Chandrasekhar, V. Heterometallic Heptanuclear [Cu₅Ln₂] (Ln = Tb, Dy, and Ho) Single-Molecule Magnets Organized in One-Dimensional Coordination Polymeric Network. *Inorg. Chem.* **2017**, 56, 14612–14623. (g) Vidick, D.; Ke, X.; Devillers, M.; Poleunis, C.; Delcorte, A.; Moggi, P.; Van Tendeloo, G.; Hermans, S. Heterometal nanoparticles from Ru-based molecular clusters covalently anchored onto functionalized carbon nanotubes and nanofibers. *Beilstein J. Nanotechnol.* **2015**, 6, 1287–1297.
- (2) Buchwalter, P.; Rosé, J.; Braunstein, P. Multimetallic Catalysis Based on Heterometallic Complexes and Clusters. *Chem. Rev.* **2015**, 115, 28–126.
- (3) (a) Stolarov, I. P.; Yakushev, I. A.; Dorovatovskii, P. V.; Zubavichus, Y. V.; Khrustalev, V. N.; Vargaftik, M. N. First platinum(II)–alkaline-earth acetate-bridged complexes PtII(μ-OAc)-4MII(AcOH)₄ (M = Ca, Sr, Ba). *Mendeleev Commun.* **2018**, 28, 200–201. (b) Kozitsyna, N. Yu.; Nefedov, S. E.; Yakushev, I. A.; Dobrokhotova, Zh. V.; Vargaftik, M. N.; Moiseev, I. I. Synthesis, crystal structure and thermal redox transformations of palladium(II)–alkaline earth tetraacetate-bridged lantern complexes PdII(μ-OOCMe)₄MII(HOOCMe)₄ (M = Ca, Sr, Ba). *Mendeleev Commun.* **2007**, 17, 261–263.

(4) (a) van der Ploeg, A. F. M. J.; van Koten, G.; Vrieze, K. Synthesis of Novel Binuclear Palladium–Thallium Carboxylates of the Type PdTl(O₂CR)₅ and their Structural Characterization Based on Observation of J(^{203–205}Tl–¹H) and J(^{203–205}Tl–¹³C). *Inorg. Chim. Acta* **1980**, *38*, 253–261. (b) Balch, A. L.; Davis, B. J.; Fung, E. Y.; Olmstead, M. M. Palladium–thallium interactions in dinuclear complexes with structural components that place the two metal centers in close proximity. *Inorg. Chim. Acta* **1993**, *212*, 149–156.

(5) (a) Aldridge, S. The Chemistry of the Group 13 Metals in the +3 Oxidation State: Simple Inorganic Compounds. In *The Group 13 Metals Aluminium, Gallium, Indium and Thallium: Chemical Patterns and Peculiarities*; Aldridge, S., Downs, A. J., Eds.; John Wiley & Sons, 2011; pp 75–147. (b) Bradley, S. M.; Kydd, R. A.; Yamdagni, R. Comparison of the Hydrolyses of Gallium(III) and Aluminium(III) Solutions by Nuclear Magnetic Resonance Spectroscopy. *J. Chem. Soc., Dalton Trans.* **1990**, 2653–2656. (c) Mensinger, Z. L.; Zakharov, L. N.; Johnson, D. W. Synthesis and Crystallization of Infinite Indium and Gallium Acetate 1D Chain Structures and Concomitant Ethyl Acetate Hydrolysis. *Inorg. Chem.* **2009**, *48*, 3505–3507.

(6) (a) Kozitsyna, N. Yu.; Nefedov, S. E.; Cherkashina, N. V.; Ikorskii, V. N.; Vargaftik, M. N.; Moiseev, I. I. First crystalline palladium(II) carboxylate complex with divalent 3d metal, PdCo(μ-OOCMe)₄(NCMe): synthesis and structure. *Russ. Chem. Bull.* **2005**, *54*, 2215–2218. (b) Kozitsyna, N. Yu.; Nefedov, S. E.; Dolgushin, F. M.; Cherkashina, N. V.; Vargaftik, M. N.; Moiseev, I. I. Heterodimetallic Pd^{II}-based Carboxylate-Bridged Complexes: Synthesis and Structure of Single-Crystalline Pd^{II}-M (M = Mn^{II}, Co^{II}, Ni^{II}, Cu^{II}, Zn^{II}, Nd^{III}, Eu^{III}, Ce^{IV}) acetates. *Inorg. Chim. Acta* **2006**, *359*, 2072–2086. (c) Tkachenko, O. P.; Stakheev, A. Yu.; Kustov, L. M.; Mashkovsky, I. V.; van den Berg, M.; Grünert, W.; Kozitsyna, N. Yu.; Dobrokhotova, Zh. V.; Zhilov, V. I.; Nefedov, S. E.; Vargaftik, M. N.; Moiseev, I. I. An easy way to Pd–Zn nanoalloy with defined composition from a heterobimetallic Pd(μ-OOCMe)₄Zn(OH₂) complex as evidenced by XAFS and XRD. *Catal. Lett.* **2006**, *112*, 155–161. (d) Akhmadullina, N. S.; Cherkashina, N. V.; Kozitsyna, N. Yu.; Stolarov, I. P.; Perova, E. V.; Gekhman, A. E.; Nefedov, S. E.; Vargaftik, M. N.; Moiseev, I. I. Synthesis of palladium(II)–3d-metal(II) paddlewheel acetate-bridged heterodimetallic complexes: unexpected catalysis by water molecules. *Inorg. Chim. Acta* **2009**, *362*, 1943–1951. (e) Kozitsyna, N. Yu.; Nefedov, S. E.; Klyagina, A. P.; Markov, A. A.; Dobrokhotova, Zh. V.; Velikodny, Yu. A.; Kochubey, D. I.; Zyubina, T. S.; Gekhman, A. E.; Vargaftik, M. N.; Moiseev, I. I. Novel heterometallic palladium–silver complex. *Inorg. Chim. Acta* **2011**, *370*, 382–387.

(7) (a) Kozitsyna, N. Yu.; Nefedov, S. E.; Vargaftik, M. N.; Moiseev, I. I. The first heterodimetallic palladium–rare-earth metal complexes Pd₂^{II}Sm₃^{III}(μ,η²-OOCMe)₂(μ-OOCMe)₃L₂(L = OH₂, THF): synthesis and crystal structure. *Mendeleev Commun.* **2005**, *15*, 223–224. (b) Kozitsyna, N. Yu.; Nefedov, S. E.; Dobrokhotova, Zh. V.; Ikorskii, V. N.; Stolyarov, I. P.; Vargaftik, M. N.; Moiseev, I. I. The route to heteronuclear nanoclusters from the viewpoint of coordination chemistry. *Nanotechnol. Russ.* **2008**, *3*, 166–183. (c) Nefedov, S. E.; Kozitsyna, N. Yu.; Vargaftik, M. N.; Moiseev, I. I. Palladium(II)–rare-earth metal(III) paddlewheel carboxylate complexes: Easy total acetate to pivalate metathesis. *Polyhedron* **2009**, *28*, 172–180. (d) Nefedov, S. E.; Kozitsyna, N. Yu.; Akhmadullina, N. S.; Cherkashina, N. V.; Vargaftik, M. N.; Moiseev, I. I. Unusual heterobimetallic palladium(II)–cerium(III) acetate complexes. *Inorg. Chem. Commun.* **2011**, *14*, 554–557.

(8) (a) Tsodikov, M. V.; Yandieva, F. A.; Kugel, V. Ya.; Chistyakov, A. V.; Gekhman, A. E.; Moiseev, I. I. Reductive Dehydration of Ethanol: A New Route Towards Alkanes. *Catal. Lett.* **2008**, *121*, 199–208. (b) Chistyakov, A. V.; Tsodikov, M. V.; Murzin, V. Yu.; Yandieva, F. A.; Zubavichus, Ya. V.; Kozitsyna, N. Yu.; Gekhman, A. E.; Krivtsov, V. V.; Moiseev, I. I. Cocatalytic Effect of Palladium and Zinc in the Condensation of Alcohol Carbon Backbones into Hydrocarbons. *Kinet. Catal.* **2011**, *52*, 258–272. (c) Khranov, E.; Belyakova, O.; Murzin, V.; Veligzhanin, A.; Chernyshov, A.; Vargaftik, M.; Kozitsyna, N.; Zubavichus, Y. Investigation into the Palladium–Europium Acetate Reductive Decomposition with Synchrotron Radiation-Based X-ray

Diffraction and X-ray Adsorption Spectroscopy. *Z. Anorg. Allg. Chem.* **2014**, *640*, 2577–2582. (d) Mashkovsky, I. S.; Baeva, G. N.; Stakheev, A. Yu.; Vargaftik, M. N.; Kozitsyna, N. Yu.; Moiseev, I. I. Novel Pd–Zn/C catalyst for selective alkyne hydrogenation: Evidence for the formation of Pd–Zn bimetallic alloy particles. *Mendeleev Commun.* **2014**, *24*, 355–357. (e) Markov, P. V.; Bragina, G. O.; Baeva, G. N.; Tkachenko, O. P.; Mashkovsky, I. S.; Yakushev, I. A.; Kozitsyna, N. Yu.; Vargaftik, M. N.; Stakheev, A. Yu. Pd–Cu catalysts from acetate complexes in liquid-phase diphenylacetylene hydrogenation. *Kinet. Catal.* **2015**, *56*, 591–597. (f) Rassolov, A. V.; Markov, P. V.; Bragina, G. O.; Baeva, G. N.; Mashkovskii, I. S.; Yakushev, I. A.; Vargaftik, M. N.; Stakheev, A. Yu. Catalytic properties of nanostructured Pd–Ag catalysts in the liquid-phase hydrogenation of terminal and internal alkynes. *Kinet. Catal.* **2016**, *57*, 853–858. (h) Stakheev, A. Yu.; Smirnova, N. S.; Krivoruchenko, D. S.; Baeva, G. N.; Mashkovsky, I. S.; Yakushev, I. A.; Vargaftik, M. N. *Mendeleev Commun.* **2017**, *27*, 515–517.

(9) (a) Maitlis, P. M. Metal Complexes and Catalytic Reactions. *The Organic Chemistry of Palladium*; Academic Press: New York, 1971; Vols. 1 and 2. (b) Maitlis, P. M.; Espinet, P.; Russel, M. J. H. *Comprehensive Organometallic Chemistry*; Pergamon Press: Oxford, U.K., 1982; Vol. 8. (c) Sinfelt, J. H. *Bimetallic Catalysts. Discoveries, Concepts and Applications*; Wiley: New York, 1983.

(10) Perrin, D. D.; Armarego, W. L. F. *Purification of Laboratory Chemicals*, 3rd ed.; Pergamon: Oxford, U.K., 1988.

(11) Stephenson, T. A.; Morehouse, S. M.; Powell, A. R.; Heffer, J. P.; Wilkinson, G. Carboxylates of palladium, platinum, and rhodium, and their adducts. *J. Chem. Soc.* **1965**, 3632–3640.

(12) SAINT: Area-Detector Integration Software; Bruker, Madison, WI, 2012.

(13) Batty, T. G. G.; Kontogiannis, L.; Johnson, O.; Powell, H. R.; Leslie, A. G. W. iMOSFLM: a new graphical interface for diffraction-image processing with MOSFLM. *Acta Crystallogr., Sect. D: Biol. Crystallogr.* **2011**, *67*, 271–281.

(14) Sheldrick, G. M. SADABS; Bruker AXS Inc.: Madison, WI, 1997. Evans, P. R. Scaling and assessment of data quality. *Acta Crystallogr., Sect. D: Biol. Crystallogr.* **2006**, *62*, 72–82.

(15) Sheldrick, G. M. Crystal structure refinement with SHELXL. *Acta Crystallogr., Sect. C: Struct. Chem.* **2015**, *71*, 3–8.

(16) Adamo, C.; Barone, V. Toward reliable density functional methods without adjustable parameters: The PBE0 model. *J. Chem. Phys.* **1999**, *110*, 6158–6170.

(17) Zhao, Y.; Truhlar, D. G. The M06 suite of density functionals for main group thermochemistry, thermochemical kinetics, noncovalent interactions, excited states, and transition elements: Two new functionals and systematic testing of four M06-class functionals and 12 other functionals. *Theor. Chem. Acc.* **2008**, *120*, 215–241.

(18) (a) Grimme, S.; Antony, J.; Ehrlich, S.; Krieg, H. A consistent and accurate ab initio parametrization of density functional dispersion correction (DFT-D) for the 94 elements H–Pu. *J. Chem. Phys.* **2010**, *132*, 154104. (b) Peverati, R.; Baldrige, K. K. Implementation and Performance of DFT-D with Respect to Basis Set and Functional for Study of Dispersion Interactions in Nanoscale Aromatic Hydrocarbons. *J. Chem. Theory Comput.* **2008**, *4*, 2030–2048.

(19) Schmidt, M. W.; Baldrige, K. K.; Boatz, J. A.; Elbert, S. T.; Gordon, M. S.; Jensen, J. H.; Koseki, S.; Matsunaga, N.; Nguyen, K. A.; Su, S.; Windus, T. L.; Dupuis, M.; Montgomery, J. A. General atomic and molecular electronic structure system. *J. Comput. Chem.* **1993**, *14*, 1347–1363.

(20) (a) Noro, T.; Sekiya, M.; Koga, T. Contracted polarization functions for the atoms helium through neon. *Theor. Chem. Acc.* **1997**, *98*, 25–32. (b) Sakai, Y.; Miyoshi, E.; Klobukowski, M.; Huzinaga, S. *J. Chem. Phys.* **1997**, *106*, 8084–8092. (c) Miyoshi, E.; Sakai, Y.; Tanaka, K.; Masamura, M. *J. Mol. Struct.: THEOCHEM* **1998**, *451*, 73–79. (d) Sekiya, M.; Noro, T.; Osanai, Y.; Koga, T. *Theor. Chem. Acc.* **2001**, *106*, 297–300. (e) Osanai, Y.; Sekiya, M.; Noro, T.; Koga, T. *Mol. Phys.* **2003**, *101*, 65–71. (f) Osanai, Y.; Soejima, E.; Noro, T.; Mori, H.; Mon, M. S.; Klobukowski, M.; Miyoshi, E. *Chem. Phys. Lett.* **2008**, *463*, 230–234.

(21) (a) Weigend, F.; Ahlrichs, R. *Phys. Chem. Chem. Phys.* **2005**, *7*, 3297. (b) Schuchardt, K. L.; Didier, B. T.; Elsethagen, T.; Sun, L.; Gurumoorathi, V.; Chase, J.; Li, J.; Windus, T. L. *J. Chem. Inf. Model.* **2007**, *47*, 1045–1052.

(22) *Jmol: an open-source Java viewer for chemical structures in 3D*, <http://www.jmol.org>.

(23) Ravel, B.; Newville, M. ATHENA, ARTEMIS, HEPHAESTUS: data analysis for X-ray absorption spectroscopy using IFEFFIT. *J. Synchrotron Radiat.* **2005**, *12*, 537–541.

(24) (a) Liron, F.; Oble, J.; Lorion, M. M.; Poli, G. Direct Allylic Functionalization Through Pd-Catalyzed C–H Activation. *Eur. J. Org. Chem.* **2014**, *27*, 5863–5883. (b) Moiseev, I. I.; Vargaftik, M. N. Allylic oxidation of alkenes with palladium catalysts. *Coord. Chem. Rev.* **2004**, *248*, 2381–2391. (c) Moiseev, I. I.; Gekhman, A. E.; Tsodikov, M. V.; Kugel, V. Ya.; Yandieva, F. A.; Glebov, L. S.; Kliger, G. Yu.; Mikaya, A. I.; Zaikin, V. G.; Maksimov, Yu. V.; Kochubey, D. I.; Kriventsov, V. V.; Mordovin, V. P.; Navio, J. A. Catalysis by Homo- and Heteronuclear Polymetallic Systems. In *Multimetallic Catalyst in Organic Synthesis*; Shibasaki, M., Yamamoto, Y., Eds.; Wiley-VHS: Weinheim, Germany, 2004; pp 249–290.